SAE International

2012-01-0250
Published 04/16/2012

doi:10.4271/2012-01-0250
saepcelec.saejournals.org

Development of a Path-following and a Speed Control Driver Model for an Electric Vehicle

Kiumars Jalali, Steve Lambert and John McPhee
Univ of Waterloo

ABSTRACT

A two-passenger all-wheel-drive urban electric vehicle (AUTO21EV) with four in-wheel motors and an active steering system has been designed and developed at the University of Waterloo. In order to evaluate the handling and performance of such a vehicle in the design stage and analyze the effectiveness of different chassis control systems before implementing them in the real vehicle, the simulation of a large number of different open-loop and closed-loop test maneuvers is necessary. Thus, in the simulation environment, not only is a mathematical vehicle model needed for every test maneuver, but a driver model must also be designed to simulate the closed-loop test maneuvers. The role of the driver model is to calculate the control inputs required to successfully follow a predefined path. Such a driver model can be implemented as an inverse dynamics problem or by a representation of a driver that can look ahead, preview the path, and change the steering wheel angle and acceleration or brake pedal positions accordingly. In this regard, a path-following driver model is developed in this work with an advanced path previewing technique. In addition, a gain scheduling speed control driver model is developed for the AUTO21EV, which adjusts the drive torques of the wheels to minimize the deviation between the desired and actual vehicle speeds.

CITATION: Jalali, K., Lambert, S. and McPhee, J., "Development of a Path-following and a Speed Control Driver Model for an Electric Vehicle," *SAE Int. J. Passeng. Cars - Electron. Electr. Syst.* 5(1):2012, doi:10.4271/2012-01-0250.

INTRODUCTION

The driver of a passenger car is responsible not only for controlling the vehicle speed by actuating the brake and accelerator pedals, but also for controlling the direction in which the vehicle is travelling. Thus, the tasks of the driver are threefold: navigation, path following, and vehicle stability [1]. In order to travel between two points, a driver must first choose a suitable route. Criteria such as route length and travelling time might be used to select the desired route. Navigation systems can help a driver plan a route between two points, but the ultimate decision about which route to select is still made by the driver. The second task of a driver is to define the desired path for the vehicle within the chosen route based on additional information that is gathered along the way, such as traffic conditions, traffic signs, and unexpected obstacles. Despite technical advancements in this area, the path-following task cannot be fully automated using control systems such as path-following cameras or inductive highway striping. The final task of a driver is to keep the vehicle on the desired path using the available actuators (the steering wheel, brake pedal, and accelerator pedal). Moreover, the driver is responsible for the stability of the vehicle while driving through the desired path.

From a control systems perspective, the driver and vehicle can be modelled as a control loop, where the driver acts as a controller that is responsible for the stability of the plant, which is the vehicle (Figure 1). In such a control loop, some disturbances act on the driver (such as the relative motion between the vehicle and the driver, driver distractions, and line-of-sight obstructions), and others act on the vehicle (such as cross wind, different coefficients of friction on the road, and road roughness). In terms of the lateral dynamics, the actuating variable that must be corrected by the driver is the steering wheel angle; in terms of the longitudinal dynamics, the actuating variables are the brake and accelerator pedal positions. The control deviation that must be corrected by the driver in the lateral dynamics domain is the difference between the desired and actual paths, while in the longitudinal dynamics domain, the deviation between the desired and actual speeds must be corrected. Moreover, the driver-vehicle-environment control loop is considered to be a dynamic closed-loop system, whose stability depends mostly on the vehicle behaviour and the capabilities of the driver. In other words, the stability of this control loop depends on the ability of the controller (the driver) to handle large errors, the behaviour of the control system under fast control actions,

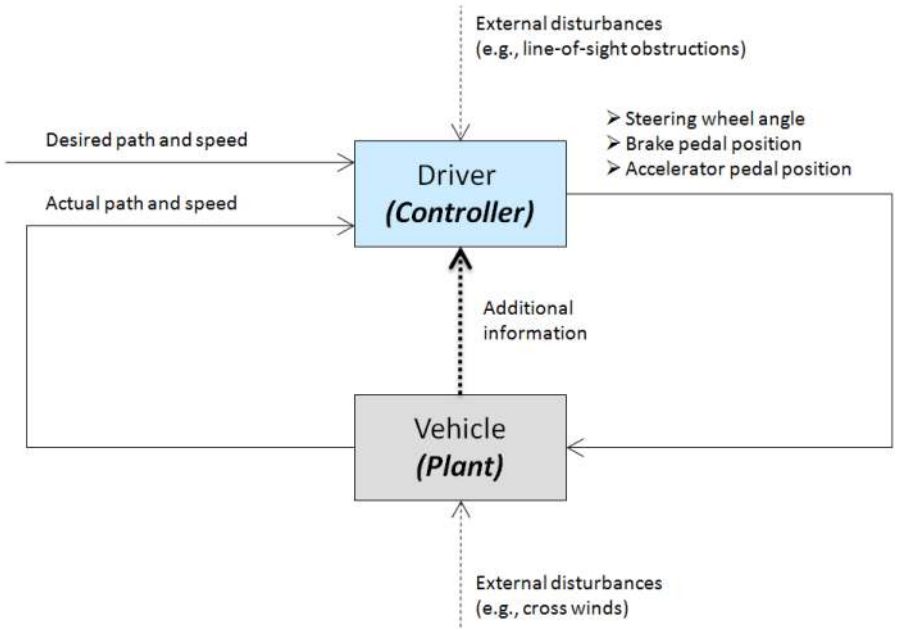

Figure 1. Graphical representation of the driver-vehicle-environment control loop

and the stability of the system under the influence of external disturbances. In general, the dynamic characteristics of the vehicle must match the capabilities of the driver. The quality of this match defines the vehicle handling and performance characteristics. In this regard, a vehicle is considered to have a good handling characteristic if the following arguments are true [1]:

• There must be a good correlation between the steering wheel variation and the lane-change behaviour of the vehicle. This property defines the transfer function behaviour of the vehicle as the plant of the control loop.

• The driver must receive reasonable information about the condition of the vehicle in order to predict its behaviour. For instance, changes in the steering wheel feedback torque, the vehicle sideslip angle, and tire squeak before reaching the physical limit of adhesion will all help the driver predict the behaviour of the vehicle and, ultimately, react correctly.

• The external disturbances acting on the vehicle should cause little or no change in the course of the vehicle - that is, the vehicle should be inherently stable.

• The vehicle must have a high lateral acceleration limit, which defines the lateral stability reserve of the vehicle; the larger this limit, the more stable the vehicle will be.

It is important to note that there are no standard legal regulations about the vehicle handling and performance characteristics, and every car manufacturer is free to set its own specifications in this area. Looking at the vehicle handling and performance from the driver's perspective, it is a completely subjective evaluation that can change from one driver to another. Therefore, it is very difficult to set a standard criterion for quantifying the quality of these evaluations. In fact, there is no comprehensive, objective definition for the dynamic characteristics associated with the driver-vehicle-environment control loop, as adequate data on the precise control characteristics of the human element are still not available [2]. For this reason, in practice, the assessment of the vehicle is performed by expert drivers who can subjectively evaluate the measured data gathered through a series of standard test maneuvers.

Figure 2 illustrates the AUTO21EV, which is a two-passenger all-wheel-drive urban electric vehicle developed and modelled in this work using the ADAMS/View environment. This vehicle has a similar configuration to the commercially available Smart *fortwo*, but it is equipped with four direct-drive in-wheel motors and an active steering system on the front axle. Further details about AUTO21EV can be found in [3]. In order to evaluate the handling and performance of the AUTO21EV and analyze the effectiveness of different chassis control systems before implementing them in the real vehicle, the simulation of a large number of different test maneuvers is necessary. In this regard, in the simulation environment, not only is a mathematical vehicle model needed for every test maneuver, but a driver model must also be designed to simulate the closed-loop test maneuvers.

DIFFERENT TEST MANEUVERS FOR EVALUATING VEHICLE HANDLING AND PERFORMANCE

Many test maneuvers have been developed for evaluating the quality of the handling and performance characteristics of a vehicle. Many of these test maneuvers are based on ideal driving conditions, and some of them are motivated by the

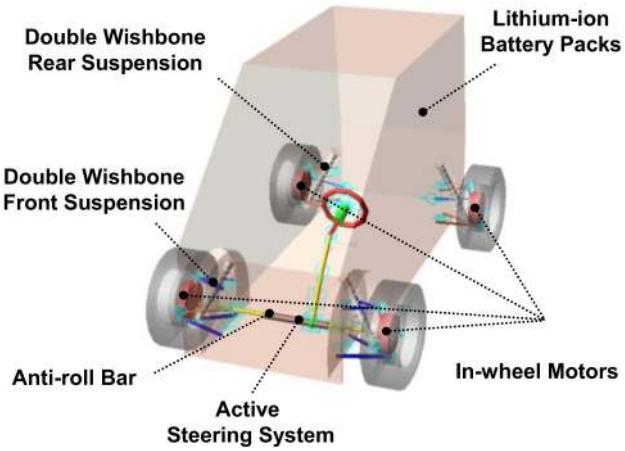

Figure 2. AUTO21EV concept vehicle

Driving Situation	Test Maneuvers	Closed-loop	Open-loop
Cornering Events	Steady-state constant radius cornering	N	Y
	Load-cycle changes	Y	Y
	Transient constant radius cornering	Y	Y
	Braking-in-turn	Y	Y
	Aquaplaning (μ-split road)	Y	Y
Straight-line Events	Directional stability	Y	Y
	Straight-line acceleration	Y	Y
	Aquaplaning (μ-split road)	Y	Y
	Straight-line braking	Y	Y
	Cross wind	Y	Y
	Load-cycle changes	Y	Y
	Responsiveness test	Y	N
Dynamic Performance Tests	Step-steer	N	Y
	Impulse-steer	N	Y
	Single-lane-change	Y	N
	ISO double-lane-change	Y	N
	Driving in a curve	Y	N
	Driving out of a curve	Y	N
Transient Behaviour Tests	Sine steer	N	Y
	Swept-sine steer	Y	N
	Step-steer and acceleration	N	Y
	Obstacle avoidance test	Y	N

Figure 3. Different test maneuvers for evaluating vehicle handling and performance characteristics [4] (Y = yes and N = no)

examination methods typically used for control systems, such as step-steer and swept-sine-steer maneuvers (Figure 3). An extensive overview of different test maneuvers and their detailed descriptions can be found in the publications of Roenitz, Braess, and Zomotor [4, 5].

The test maneuvers that describe the vehicle behaviour in terms of the driver-vehicle-environment control loop are known as ‘closed-loop’ test maneuvers. To evaluate these maneuvers, the quality of the match between the dynamic behaviour of the vehicle and the driver's capabilities must be considered. These test maneuvers require a professional driver who can make judgments on the handling qualities of the vehicle based on the combination of diverse subjective impressions. In the simulation environment, an appropriate driver model is used simulating the required behaviour of a specific driver (professional or average driver) in following a desired predefined path, in place of a test driver.

On the other hand, if the actuation variables in a test maneuver are defined to be pure functions of time, and the dynamic behaviour of the vehicle has no influence on the driver's response, then the test maneuver is known as an ‘open-loop’ maneuver. In an open-loop test maneuver, the driver is replaced by a specific, objectively quantifiable interference factor, and the handling data derived from the maneuver provides objective information about the handling qualities of the vehicle. Open-loop test maneuvers also provide insight into the stability of the vehicle and the sensitivity of the vehicle to external disturbances. In

summary, each test maneuver provides some information about the dynamic behaviour of the vehicle in one or several respects, such as vehicle handling, stability, path following, and longitudinal dynamics. Therefore, a comprehensive evaluation of the dynamic characteristics of a vehicle is only possible by examining the results obtained from several different test maneuvers.

MODELLING THE BEHAVIOUR OF A DRIVER

In order to evaluate the handling and performance of the vehicle in the design stage and the effectiveness of different chassis control subsystems before implementing them in a real vehicle, the simulation of a large number of different maneuvers is necessary. As discussed earlier, there is a significant difference between open-loop test maneuvers, which are defined by chronological control inputs and are routinely used for the subjective evaluation of handling performance, and closed-loop test maneuvers, which primarily involve a path-following task. However, in order to realize these test maneuvers in the simulation environment, not only is a mathematical vehicle model needed for every test maneuver, but a driver model must also be designed to simulate the closed-loop test maneuvers. The role of the driver model is to calculate the control inputs required to successfully follow a predefined path. Such a driver model can be implemented as an inverse dynamics problem [6] or by a representation of a driver that can look ahead, preview the path, and change the steering wheel angle accordingly [7, 8].

There exist a variety of controllers suitable for modelling driver behaviour, some of which are more complex than the others. Therefore, one should first choose the level of modelling fidelity required to achieve the task at hand, based on the needs of the simulation. In general, driver models fall into two main categories: optimum control models and moment-by-moment feedback models [9]. Optimum control models use some form of penalty function as a measure to assess the quality of the control achieved. These models use repeated simulations of a specific event and numerical optimization methods to tune the parameters of the driver model such that the value of the defined penalty function is minimized over the duration of the event of interest. Although optimum control models are suitable for learned events, such as the circuit driving of race cars, some care must be exercised with their use for evaluating the performance of regular passenger cars. Since the average driver of a passenger vehicle is generally unskilled, the application of modelling techniques in which repeated simulations are used to discover the so-called 'best' way of achieving a maneuver may not be an appropriate way of simulating an emergency situation, where the driver has only one attempt to complete the maneuver [7, 10]. Moment-by-moment feedback models are a subset of the optimum control models, with the difference being that the feedback parameters of the controller are set once by the analyst and remain constant thereafter. Although these models are less appropriate for predicting the driver behaviour for circuit racing, they add clarity in understanding the vehicle behaviour and driver inputs when driving through a test maneuver [11]. Such driver models are also more appropriate for understanding the effects of different chassis control systems on both the vehicle and the driver when driving through closed-loop test maneuvers.

DEVELOPMENT OF A PATH-FOLLOWING DRIVER MODEL

With these facts in mind, a moment-by-moment feedback driver model that is similar to the model described in [8] is developed in this work, but is enhanced with a more sophisticated path previewing technique. The driver model described in [8] uses a single-preview-point steering control model, whose objective is to steer a ground vehicle along a reference line located in the middle of the lane to be followed. In this regard, a single arbitrary look-ahead point is defined along the local longitudinal axis of the vehicle, and the distance between the look-ahead point and the reference path is defined as the "look-ahead offset". The required steer angle is then calculated as a function of the look-ahead offset, vehicle longitudinal velocity, and various vehicle parameters. A linear bicycle model is used, as illustrated in Figure 4, to obtain the following linear state-space equation [8]:

$$\begin{bmatrix}\dot{v}\\ \dot{r}\end{bmatrix}=\begin{bmatrix}-\dfrac{C_{\alpha f}+C_{\alpha r}}{m_{CG}\cdot u} & -u+\dfrac{b\cdot C_{\alpha r}-a\cdot C_{\alpha f}}{m_{CG}\cdot u}\\ \dfrac{b\cdot C_{\alpha r}-a\cdot C_{\alpha f}}{I_z\cdot u} & -\dfrac{a^2\cdot C_{\alpha f}+b^2\cdot C_{\alpha r}}{I_z\cdot u}\end{bmatrix}\cdot\begin{bmatrix}v\\ r\end{bmatrix}+\begin{bmatrix}\dfrac{C_{\alpha f}}{m_{CG}}\\ \dfrac{a\cdot C_{\alpha f}}{I_z}\end{bmatrix}\cdot\delta \quad (1)$$

where u, v, and r are, respectively, the longitudinal, lateral, and yaw rate vectors of the vehicle, and $u=|\vec{u}|$, $v=|\vec{v}|$, and $r=\dot{\psi}=|\vec{r}|$ are the magnitudes of these vectors. In addition, a and b are the distances of the front and rear axles to the vehicle center of gravity, m_{CG} is the vehicle mass, I_z is the yaw moment of inertia, δ is the steering angle of the front wheel, and $C_{\alpha f}$ and $C_{\alpha r}$ are the total cornering stiffnesses of the front and rear tires, respectively. As illustrated in Figure 4, $\vec{V}$ indicates the velocity vector of the vehicle's center of gravity, whose magnitude is $V=|\vec{V}|=\sqrt{u^2+v^2}$. Note that the vehicle coordinate axes are in accordance with the ISO 4130 and DIN 70000 standards, where the Z direction points upwards, the X-axis is along the vehicle longitudinal axis and points towards the front of the vehicle, and the Y-axis points left when viewing along the positive X direction.

Figure 5 illustrates the vehicle motion along a desired circular path of radius R, where the distance between the

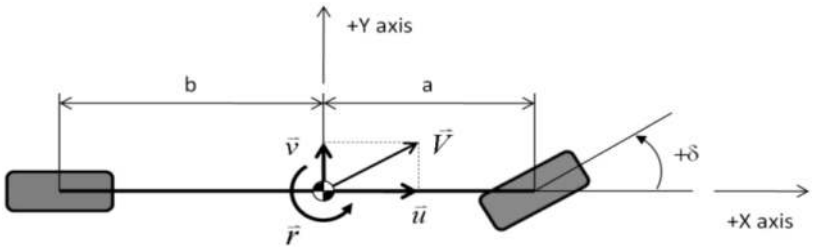

Figure 4. Linear bicycle model used for developing the driver model

center of gravity of the vehicle and the look-ahead point is defined as look-ahead distance *d*, the distance between the look-ahead point and the point on the curve closest to it is defined as look-ahead offset *o*, and the distance between the look-ahead point and the center of the curve is defined as *h*. By considering the steady-state motion of the vehicle along the curve, where the vehicle perfectly tracks the desired path, explicit expressions are obtained for the variables v_{ss}, r_{ss}, V_{ss}, δ_{ss}, o_{ss}, and h_{ss}. All of these expressions are in terms of the vehicle longitudinal speed *u*, the radius of curvature *R*, and the vehicle parameters. Note that the subscript '*ss*' indicates that the values are calculated when the vehicle is in a steady-state condition, where $\dot{v} = \dot{r} = 0$, the center of gravity of the vehicle perfectly tracks the desired curve, the velocity vector *V* is tangent to the curve, and the longitudinal velocity *u* is held constant. At steady-state, equation (1) becomes the following:

$$-\begin{bmatrix} -\dfrac{C_{\alpha f}+C_{\alpha r}}{m_{CG}\cdot u} & -u+\dfrac{b\cdot C_{\alpha r}-a\cdot C_{\alpha f}}{m_{CG}\cdot u} \\ \dfrac{b\cdot C_{\alpha r}-a\cdot C_{\alpha f}}{I_z\cdot u} & -\dfrac{a^2\cdot C_{\alpha f}+b^2\cdot C_{\alpha r}}{I_z\cdot u} \end{bmatrix}\cdot\begin{bmatrix} v_{ss} \\ r_{ss} \end{bmatrix}=\begin{bmatrix} \dfrac{C_{\alpha f}}{m_{CG}} \\ \dfrac{a\cdot C_{\alpha f}}{I_z} \end{bmatrix}\cdot\delta_{ss} \tag{2}$$

From equation (2), the steady-state lateral velocity (v_{ss}) can be calculated as a function of the steady-state yaw rate (r_{ss}) as follows [8]:

$$v_{ss} = T\cdot r_{ss},\ \text{where}\ T = b-\frac{a\cdot m_{CG}\cdot u^2}{C_{\alpha r}\cdot(a+b)} \tag{3}$$

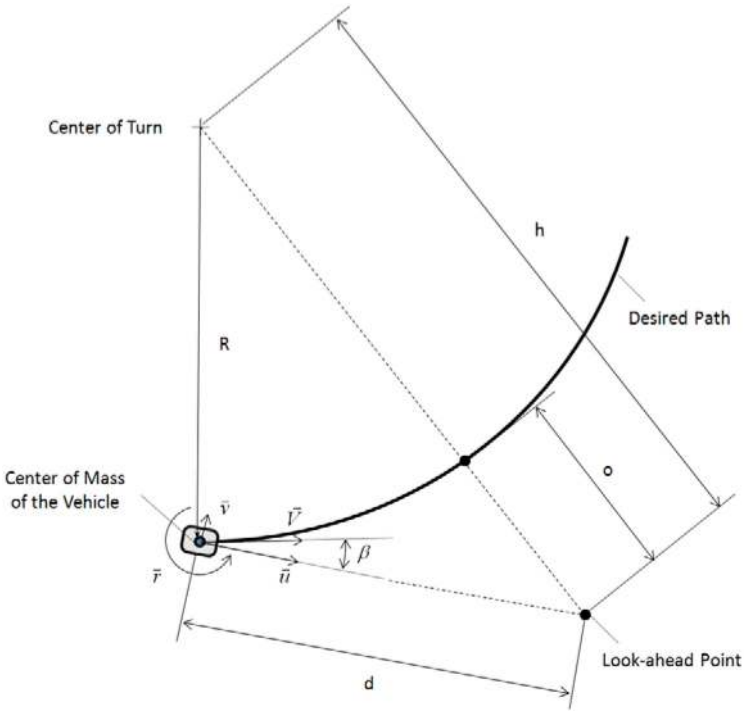

Figure 5. Steady-state vehicle motion along a circular path of radius R

In general, the following statements can be made for a vehicle in steady-state circular motion [8]:

$$V_{ss} = \sqrt{u^2+v_{ss}^2} \tag{4}$$

$$V_{ss} = R\cdot r_{ss} \tag{5}$$

One can now obtain new expressions for r_{ss} and δ_{ss} from equations (2), (3), (4), (5) that are only in terms of the vehicle longitudinal speed *u*, the radius of curvature *R*, and vehicle parameters [8]:

$$r_{ss} = \frac{u}{\sqrt{R^2-T^2}} \tag{6}$$

$$\delta_{ss} = \frac{1}{\sqrt{R^2 - T^2}} \cdot \left(a + b - \frac{m_{CG} \cdot u^2 \cdot \left(a \cdot C_{\alpha f} - b \cdot C_{\alpha r} \right)}{(a+b) \cdot C_{\alpha f} \cdot C_{\alpha r}} \right) \quad (7)$$

According to equation (3), the largest value for T is always less than b, which is the distance of the rear axle to the vehicle center of gravity. Since, in reality, a vehicle with front steering system can never have a radius of curvature less than its wheelbase, equations (6) and (7) will never encounter a singularity problem.

In order to calculate an appropriate expression for the steady-state look-ahead offset o_{ss}, where o_{ss}= h_{ss} - R, an expression for h_{ss} is first defined as follows [8]:

$$h_{ss} = \sqrt{d^2 + R^2 - 2R \cdot d \cdot \cos\left(\frac{\pi}{2} + \beta\right)} = \sqrt{d^2 + R^2 - 2R \cdot d \cdot \frac{v_{ss}}{V_{ss}}} \quad (8)$$

Using equations (3), (5), and (8), the final expressions for h_{ss} and o_{ss} are obtained as follows [8]:

$$h_{ss} = \sqrt{d^2 + R^2 + 2 \cdot d \cdot T} \quad (9)$$

$$o_{ss} = \sqrt{d^2 + R^2 + 2 \cdot d \cdot T} - R \quad (10)$$

Finally, from equations (7) and (10), the ratio between the desired steering input δ_{ss} and the look-ahead offset o_{ss} is calculated as follows [8]:

$$\frac{\delta_{ss}}{o_{ss}} = \frac{\frac{1}{\sqrt{R^2 - T^2}} \cdot \left(a + b - \frac{m_{CG} \cdot u^2 \cdot \left(a \cdot C_{\alpha f} - b \cdot C_{\alpha r} \right)}{(a+b) \cdot C_{\alpha f} \cdot C_{\alpha r}} \right)}{\sqrt{R^2 + d^2 + 2 \cdot d \cdot T} - R} \quad (11)$$

At this point, two important assumptions are made by the authors of [8] in order to simplify equation (11). First, using Taylor's expansion:

$$\forall x, \varepsilon \in \mathbb{R},\ x > 0:\ \text{if } \frac{|\varepsilon|}{x} \ll 1 \Rightarrow \sqrt{x + \varepsilon} = \sqrt{x} + \frac{\varepsilon}{2\sqrt{x}} \quad (12)$$

and assuming that $\frac{|d \cdot (d + 2 \cdot T)|}{R} \ll 1$, equation (11) can be rewritten as follows [8]:

$$\frac{\delta_{ss}}{o_{ss}} = \frac{2 \cdot \left(a + b - \frac{m_{CG} \cdot u^2 \cdot \left(a \cdot C_{\alpha f} - b \cdot C_{\alpha r} \right)}{(a+b) \cdot C_{\alpha f} \cdot C_{\alpha r}} \right)}{\sqrt{1 - \frac{T^2}{R^2}} \cdot d \cdot (d + 2 \cdot T)} \quad (13)$$

Next, by assuming that $\frac{|T|}{R} \ll 1$ and, thus, $\sqrt{1 - \frac{T^2}{R^2}} \approx 1$, equation (13) can be further simplified as follows [8]:

$$\delta_{ss} \approx \frac{2 \cdot \left(a + b - \frac{m_{CG} \cdot u^2 \cdot \left(a \cdot C_{\alpha f} - b \cdot C_{\alpha r} \right)}{(a+b) \cdot C_{\alpha f} \cdot C_{\alpha r}} \right)}{d \cdot (d + 2 \cdot T)} \cdot o_{ss} \quad (14)$$

Equation (14) indicates that the steering angle required to keep the vehicle on a circular path when in steady-state motion is a function of the look-ahead offset o_{ss}, the vehicle longitudinal velocity u, the look-ahead distance d, and various vehicle parameters. It is important to notice that equation (14) is independent of the radius of curvature R, which makes it attractive for use in a driver model that is suitable for every possible road profile. Moreover, since equation (14) is a function of vehicle forward velocity, it updates itself as the vehicle speed changes, as in a gain scheduling controller. Notably, the stability of this steering controller has been proven analytically in [8] by considering a sufficiently large look-ahead distance and using the well-known Routh-Hurwitz technique.

Many researchers believe that using a single preview point for describing a driver model is unrealistic and, therefore, unsatisfactory [7, 10, 11]. If the look-ahead point is too far in front of the vehicle, it will be inappropriate to act on the preview information at the time of its acquisition, and the information has been lost by the time it is useful. On the other hand, if the look-ahead point is too close to the vehicle, it necessarily causes very poor control, especially at higher speeds. Moreover, if the road profile is complex, a single-preview-point model can result in a situation where its information does not coincide with the current state of the vehicle, even with a proper look-ahead distance (Figure 6-a). Realistically, one cannot imagine that a human driver only uses the information from a single look-ahead point in order to make an appropriate decision on how to adjust the steering wheel.

In order to solve this problem, the single-preview-point driver model described by equation (14) is enhanced in this work by taking two additional steps. First, the look-ahead distance is redefined to be a function of the vehicle longitudinal velocity and the driver's reaction time, as described in the following:

$$d_{look-ahead}(t) = d_{const} + t_{driver} \cdot u(t) \quad (15)$$

where d_{const} is a constant distance that the driver will look ahead, even at lower velocities, t_{driver} is the reaction time of the driver, and u is the vehicle longitudinal velocity. Notably, the constant distance that the driver looks ahead is chosen to be 4 meters and the reaction time of the driver is set to be 0.7

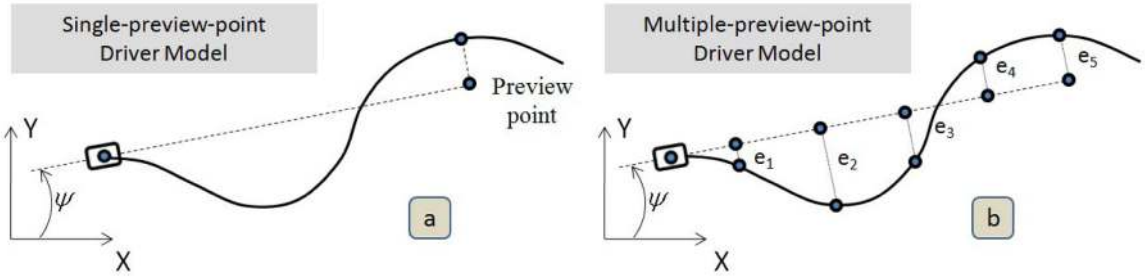

Figure 6. (a) Single-preview-point and (b) multiple-preview-point driver models

seconds. Equation (15) indicates that the faster the vehicle is driven, the longer the look-ahead distance will be, which corresponds well with the reaction of a real driver. In the second step, five preview points are defined on the "optical lever" of the driver, which is along the local longitudinal axis of the vehicle, between the vehicle center of gravity and the look-ahead distance. The coordinates of the preview points on the optical lever of the driver are calculated as follows [11]:

$$\begin{cases} x_{pp,i}(t) = x_{CG}(t) + K_i \cdot d_{look-ahead}(t) \cdot \cos(\psi(t)) \\ y_{pp,i}(t) = y_{CG}(t) + K_i \cdot d_{look-ahead}(t) \cdot \sin(\psi(t)) \end{cases} \quad (16)$$

where $x_{pp,i}(t)$ and $y_{pp,i}(t)$ are the coordinates of the i^{th} preview point, and $x_{CG}(t)$ and $y_{CG}(t)$ define the coordinates of the vehicle center of gravity at time t in the global reference frame, respectively. K_i is the relative distance between the i^{th} preview point and the vehicle center of gravity on the optical lever, $d_{look-ahead}(t)$ is the look-ahead distance defined in equation (15), and $\psi(t)$ is the vehicle yaw angle at time t. The lateral offset of each preview point from its corresponding point on the desired path is calculated as the distance between the preview point and the desired path, measured along a line that is perpendicular to the optical lever (Figure 6-b).

The new look-ahead offset is then defined as the weighted sum of all the lateral offsets:

$$e_i(t) = \left(y_{R,i}(t) - y_{pp,i}(t)\right) \cdot \cos\left(\psi(t)\right) \cdots - \left(x_{R,i}(t) - x_{pp,i}(t)\right) \cdot \sin\left(\psi(t)\right) \quad (17)$$

$$o(t) = \sum_{i=1}^{5} \left(G_i \cdot e_i(t)\right) \quad (18)$$

where $e_i(t)$ is the lateral offset, $x_{R,i}(t)$ and $y_{R,i}(t)$ are the coordinates of the intersection between the line perpendicular to the optical lever and the desired path, and G_i is the control gain of the i^{th} preview point. Note that the control gains of the driver model are derived in an ad hoc fashion based on intuition, not on any formal optimization scheme. The following control gains are chosen for the driver model: $G_1 = 3$, $G_2 = 5$, $G_3 = 4$, $G_4 = 1$, and $G_5 = 0.5$. The new driver model is described by combining equations (14) and (18) as follows:

$$\delta_{ss}(t) = \frac{2 \cdot \left(a + b - \frac{m_{CG} \cdot u^2(t) \cdot \left(a \cdot C_{\alpha f} - b \cdot C_{\alpha r}\right)}{(a+b) \cdot C_{\alpha f} \cdot C_{\alpha r}} \right)}{d_{look-ahead}(t) \cdot \left(d_{look-ahead}(t) + 2 \cdot \left(b - \frac{a \cdot m_{CG} \cdot u^2(t)}{C_{\alpha r} \cdot (a+b)} \right) \right)} \cdots \cdot \sum_{i=1}^{5} \left(G_i \cdot e_i(t)\right) \quad (19)$$

It is important to note that one can also add an orientation error, the error between the desired and actual vehicle yaw angles, to equation (18) in order to make the steering input of the driver model a function of position error as well as orientation error. However, in this work, only position error is considered.

DEVELOPMENT OF A SPEED-CONTROL DRIVER MODEL

As mentioned earlier, one of the tasks of a driver model is to adjust the brake and accelerator pedal positions such that the deviation between the desired and actual vehicle speeds is minimized. In order to do this, a gain scheduling PID controller is developed as the speed controller for the AUTO21EV. PID controllers are very popular and are widely used in industry because of their simple structure and robust performance in a wide range of operating conditions. The design of such controllers requires the specification of three parameters: the proportional, integral, and derivative gains. The important problem of tuning a PID controller involves finding appropriate settings for these three gains. The conventional approach to defining the PID parameters is to study a mathematical model of the dynamic system and attempt to derive a fixed set of gain parameters that are valid

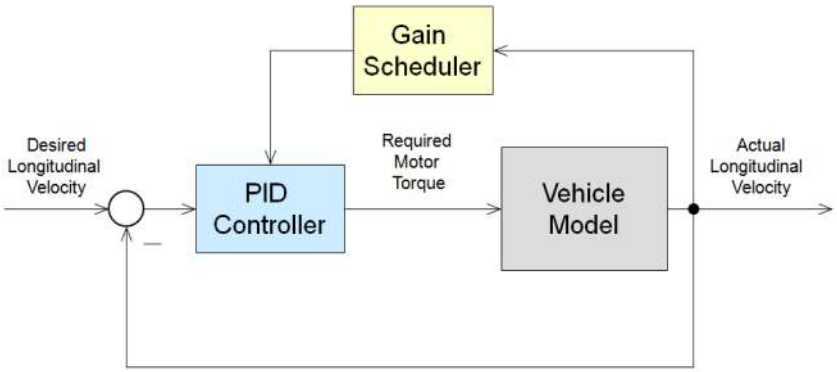

Figure 7. Block diagram of the gain scheduling speed controller

in a wide range of operating conditions. One well-known example of such an approach is the Ziegler-Nichols method [12]. Such a method works well for processes or dynamic systems that can be modelled using linear first- or second-order systems; however, most real industrial processes or dynamic systems have characteristics such as higher-order dynamics, dead-zones, or nonlinearity that make modelling them with simple linear systems inaccurate. Therefore, in the last couple of decades, there have been some efforts to find and improve tuning methods that can update the gain parameters of PID controllers at any instant based on a structurally fixed parameter-evolving process model.

One of these tuning methods is adaptive control, which uses a control scheme that is capable of modifying its behaviour in response to changes in the dynamic system. There are three well-known adaptive control schemes: gain scheduling, model-reference adaptive control, and self-tuning regulators. The gain scheduling technique is based on the adjustment of controller parameters in response to the operating conditions of a dynamic system. This type of control system is particularly useful when the variations in the dynamic system are predictable and when the control parameters need to be adjusted quickly in response to these variations [13]. Figure 7 shows a block diagram of the gain scheduling speed controller developed in this work. As shown in the figure, the difference between the driver's speed request and the actual vehicle speed is measured and amplified by the PID controller at each time step; the PID controller then outputs the required motor torque at each wheel accordingly. At this stage, it is assumed that the torque calculated by the gain scheduling speed controller ($T_{Driver,req}$) is applied to each wheel. In other words, the total amount of torque that is applied to the vehicle is equal to the following:

$$T_{total} = 4 \times T_{Driver,req} \tag{20}$$

In this case, the required motor torque ($T_{Driver,req}$) is the input to the in-wheel motor controller described in [14]. However, it is important to note that the required motor torque at each wheel may be modified by the advanced slip controller and/or the advanced torque vectoring system, which are described in [Jal10], depending on the traction potential of the tire or the vehicle driving dynamics.

The proportional (K_P^*), integral (K_I^*), and derivative (K_D^*) gains of the gain scheduling PID controller are all defined to be proportional to the vehicle forward speed, as follows:

$$K_P^* = K_P \cdot u_{act} + 5 \tag{21}$$

$$K_I^* = K_I \cdot u_{act} \tag{22}$$

$$K_D^* = K_D \cdot u_{act} \tag{23}$$

where $K_P = 70$, $K_I = 0.05$, and $K_D = 0.05$ are constant gains and u_{act} is the actual longitudinal speed of the vehicle. Notably, the proportional gain K_P^* has a constant portion, which accounts for the case that the vehicle is not moving. The following equation describes the output of the gain scheduling PID controller:

$$T_{req}(t) = K_P^* \cdot e + K_I^* \cdot \int e \cdot dt + K_D^* \cdot \frac{de}{dt} \tag{24}$$

where $e = u_{des} - u_{act}$ is the difference between the desired (u_{des}) and actual (u_{act}) vehicle speed. Since the proposed gain scheduling PID controller is part of a digital control system, the derivative and integral parts of the controller are approximated as follows:

$$\int_{t-T_s}^{t} e \cdot dt \approx \frac{1}{2}\left(e(t) + e(t-T_s)\right) \cdot T_s \tag{25}$$

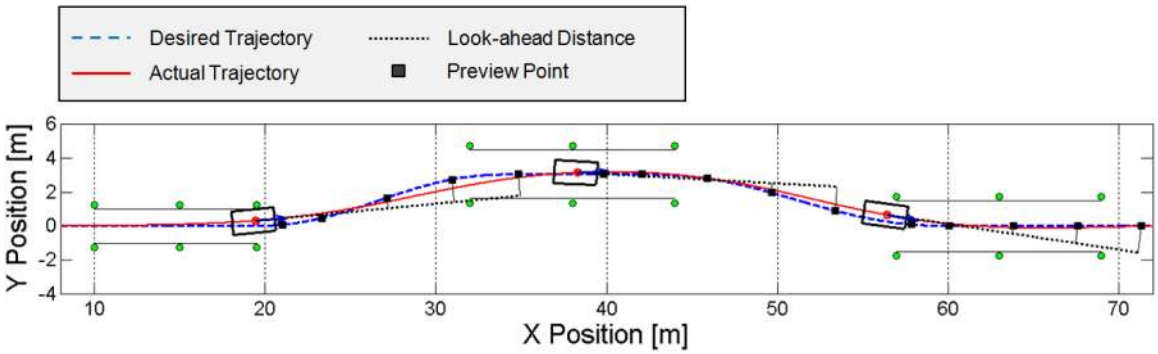

Figure 8. Path-following driver model concept in a double-lane-change maneuver

$$\frac{de}{dt} \approx \frac{e(t) - e(t - T_s)}{T_s} \tag{26}$$

where t is the current simulation time and T_S is the sampling time. It is important to notice that the controller gain parameters, namely K_P, K_I, and K_D, are tuned manually using a trial-and-error approach such that a sufficiently fast response with no overshoot is obtained over the entire speed range.

EVALUATION OF THE PATH-FOLLOWING AND SPEED-CONTROL DRIVER MODELS

The performance of the proposed path-following driver model, described in equation (19), is evaluated using two test maneuvers. First, a severe ISO double-lane-change maneuver with obstacle avoidance is used to evaluate the performance of the driver model. The ISO double-lane-change maneuver is a closed-loop test maneuver typically used to adjust the dynamics of a vehicle based on the subjective evaluations of professional drivers. In addition, the complexity of the course used in this maneuver is a good example for demonstrating the performance of the path-following driver model.

Figure 8 illustrates the concept behind the path-following driver model. At each time step, the driver model looks ahead along the vehicle longitudinal axis and calculates the look-ahead offset as the weighted sum of five lateral offsets. As mentioned earlier, each lateral offset is calculated as the distance between the preview point and the desired path measured along a line that is perpendicular to the optical lever. Using equation (19), the driver model changes the steering wheel angle based on the look-ahead offset, the vehicle longitudinal speed, the look-ahead distance, and vehicle parameters.

Figure 9-a illustrates the vehicle trajectory when driving through the double-lane-change maneuver at 40 km/h. In this simulation, the AUTO21EV vehicle model developed in the ADAMS/View environment is used [3], which is equipped with tires using the *Pacejka* 2002 [15] tire model. The simulation time is 8 seconds with a sample time of 1 millisecond. As shown in the figure, the path-following driver model is able to steer the vehicle through the desired path such that the actual vehicle trajectory matches well with the desired one. Figure 9-b illustrates the steering wheel input applied by the driver model, and Figure 9-c shows the vehicle yaw rate with respect to the driver's steering wheel input. Note that the steering system has a gear ratio of 1:18. Figure 9-c demonstrates the handling capabilities of the vehicle, as the closer this plot is to a straight narrow line, the more the vehicle behaves like its reference bicycle model, which indicates better responsiveness of the vehicle to the driver's steering input. Looking at the vehicle yaw rate and sideslip angle shown in Figure 10, it is clear that the actual vehicle yaw rate is very close to the desired yaw rate, which is calculated using the reference bicycle model and the following equation:

$$\dot{\psi} = \frac{V}{L + \frac{m_{CG}}{L}\left(\frac{b}{C_{\alpha F}} - \frac{a}{C_{\alpha R}}\right)V^2}\delta \tag{27}$$

Moreover, the vehicle sideslip angle is very small - less than 0.4 degrees - which indicates a slight understeering behaviour of the vehicle.

In order to investigate the behaviour of the driver model in the nonlinear operating regime of the vehicle, the double-lane-change maneuver is repeated at a speed of 75 km/h. Figure 11-a illustrates the vehicle trajectory when driving through the double-lane-change maneuver. Due to the fact that the vehicle is operating at its physical limit, the path-following driver model is unable to exactly match the actual vehicle trajectory with the desired one; however, the driver model is able to keep the vehicle under control throughout the entire maneuver, using counter-steering at some points. Figure 11-b shows the driver's steering wheel input which, in comparison to that shown in Figure 9-b, is much larger. Figure 11-c illustrates the vehicle yaw rate with respect to the driver's steering wheel input, which is considered to be a handling performance figure. Comparing this plot with Figure 9-c, it is clear that the phase shift between the vehicle yaw

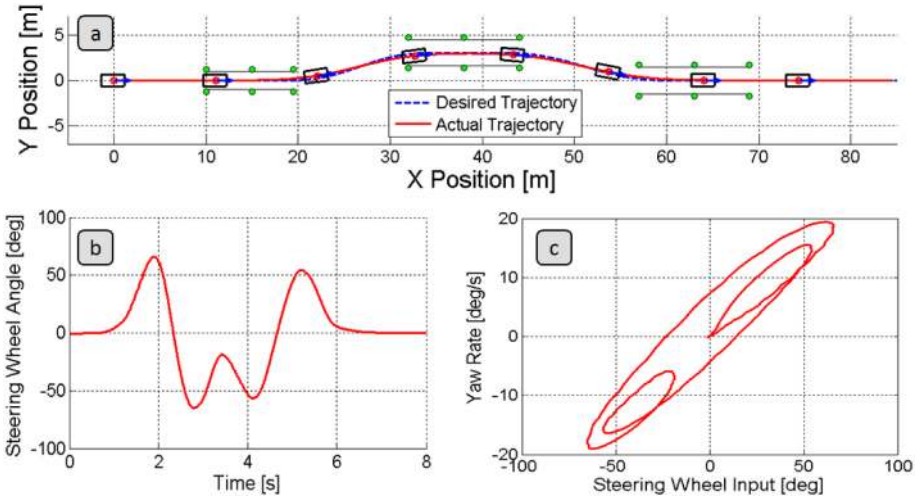

Figure 9. (a) Desired and actual vehicle trajectories, (b) driver's steering wheel input, and (c) vehicle yaw rate with respect to the steering wheel angle when driving through a double-lane-change maneuver at 40 km/h using the path-following driver model

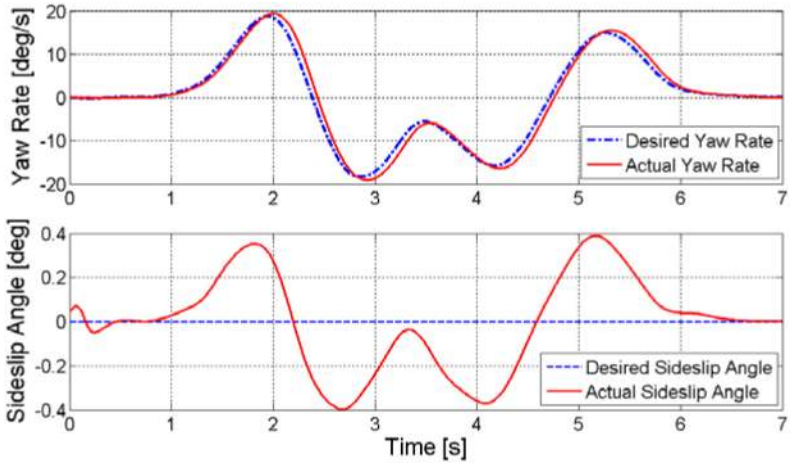

Figure 10. Desired and actual vehicle yaw rate (top) and sideslip angle (bottom) when driving through a double-lane-change maneuver at 40 km/h using the path-following driver model

rate and the driver's steering wheel input is much larger when driving through the double-lane-change maneuver at a high speed, which ultimately indicates that the vehicle responsiveness has been reduced. Figure 12 illustrates the vehicle yaw rate and sideslip angle for this maneuver, and confirms that the vehicle was operating within its physical limits.

The second test maneuver that is used to evaluate the performance of the multiple-preview-point path-following driver model is a steady-state constant radius cornering maneuver. Here, the AUTO21EV is driven through a circular path with a radius of 75 meters. The driver model attempts to keep the vehicle on the predefined path while the vehicle speed is continuously increasing from an initial speed of 5 km/h to a maximum speed of 90 km/h. As illustrated in Figure 13-a, the driver model is able to keep the vehicle on the predefined circular path even at higher velocities. Figure 13-b shows the steering wheel angle that the driver model applies to keep the vehicle on the circular path. As can be seen, the driver model continuously adjusts the steering wheel angle in order to keep the vehicle on the desired path. As the vehicle speed is increased, the driver model applies a larger steering wheel angle, thereby generating larger lateral forces on the front axle in order to compensate for the larger centripetal acceleration. Figure 13-c illustrates the desired and actual vehicle forward speeds as functions of time. This figure confirms the performance of the gain scheduling PID speed controller, as the actual vehicle speed precisely follows the driver's speed request.

The steering wheel angle applied by the driver model as a function of vehicle lateral acceleration is illustrated in Figure 14-a. It is apparent that the steering wheel angle has a linear

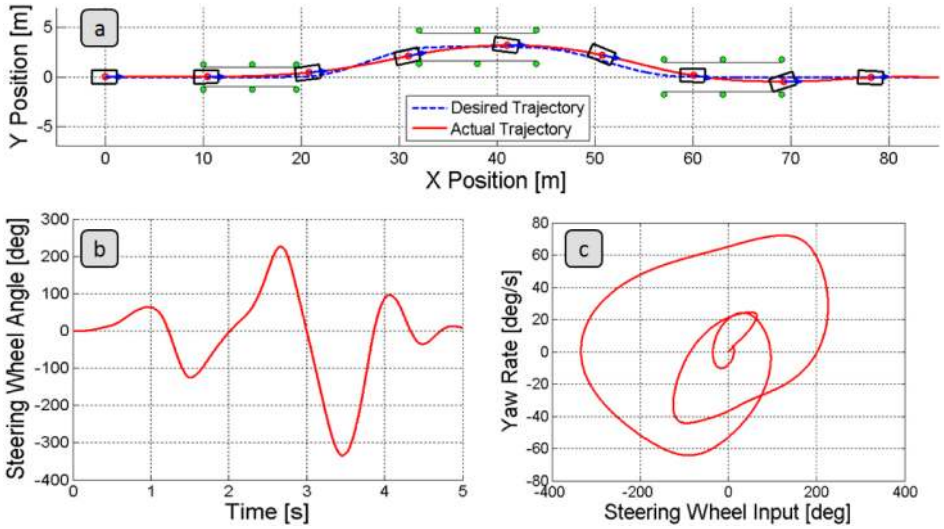

Figure 11. (a) Desired and actual vehicle trajectories, (b) driver's steering wheel input, and (c) vehicle yaw rate with respect to the steering wheel angle when driving through a double-lane-change maneuver at 75 km/h using the path-following driver model

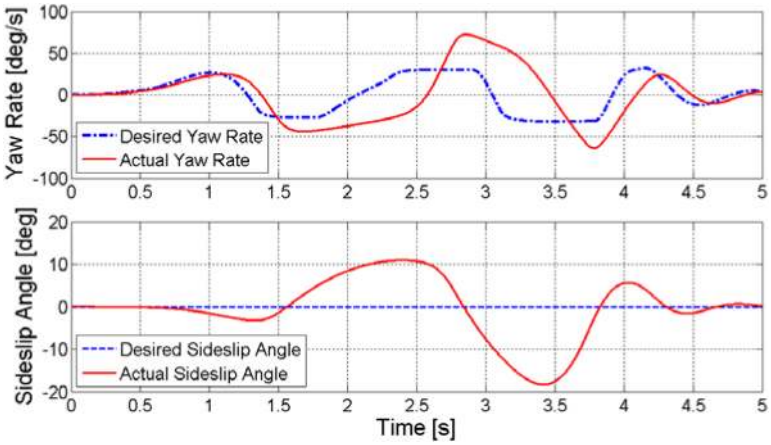

Figure 12. Desired and actual vehicle yaw rate (top) and sideslip angle (bottom) when driving through a double-lane-change maneuver at 75 km/h using the path-following driver model

gradient up to a lateral acceleration of 4 m/s^2 and then progressively increases as lateral acceleration grows. This plot very clearly indicates the understeering characteristic of the AUTO21EV. In fact, the slope of the linear region of this curve is equal to the understeering gradient of the vehicle calculated in the design stage [16]. As illustrated in Figure 14-b, the gradient of the sideslip angle is approximately linear for the majority of the lateral acceleration range, which indicates good vehicle handling. The maximum sideslip angle of the vehicle is measured as $|\beta|_{\max}$ = 5.7°, which is acceptable. Moreover, the maximum lateral acceleration is calculated to be 8.3 m/s^2, which is acceptable for a small vehicle like the AUTO21EV. This value indicates a good usage of the adhesion potential on all tires in order to keep the vehicle on its desired path. The steering ratio can be calculated as the ratio of the steering wheel angle at the beginning of the circular path (δ_{SW} = 25.8°), where the lateral acceleration is small, and the Ackermann angle $\delta_A = \frac{a+b}{R} = \frac{1.8}{75} = 1.375^\circ$ as follows:

$$i_S = \frac{\delta_{SW}}{\delta_A} = \frac{25.8^\circ}{1.375^\circ} = 18.8 \qquad (28)$$

This ratio agrees well with the steering ratio of the AUTO21EV calculated in the design stage [16].

In order to further evaluate the performance of the gain scheduling PID speed controller, the vehicle is accelerated and then braked in a stepwise speed-variation mode while driving in a straight line. In this test, the driver first increases

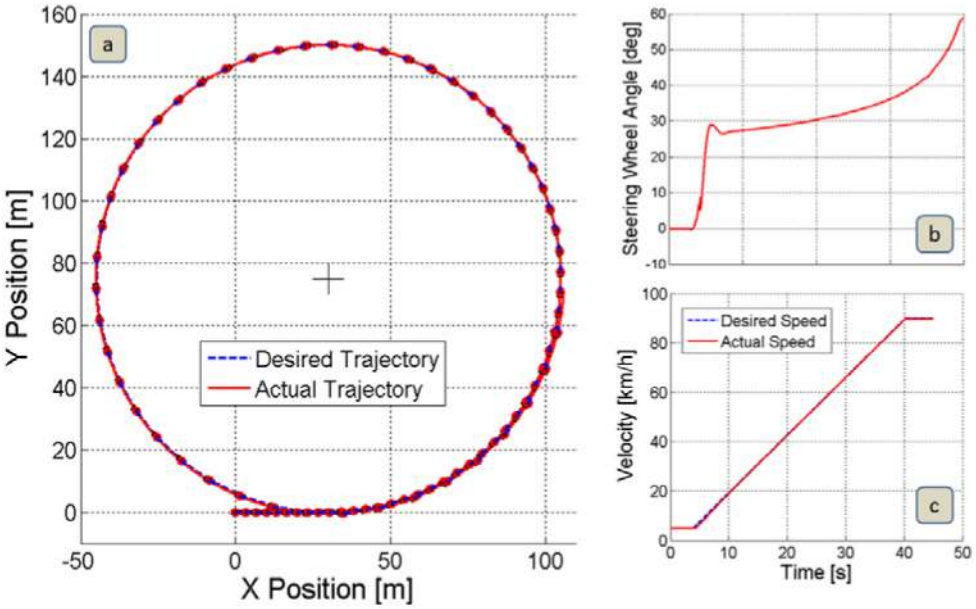

Figure 13. (a) Desired and actual vehicle trajectories, (b) required steering wheel angle applied by the driver model, and (c) desired and actual vehicle longitudinal speeds when driving through the steady-state constant radius maneuver using the path-following and speed-control driver models

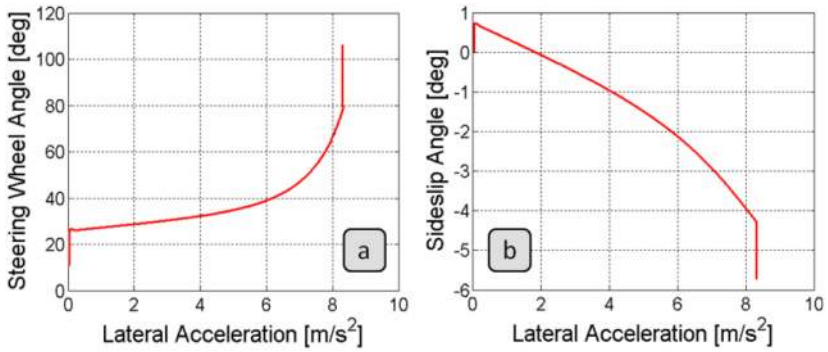

Figure 14. (a) Driver's steering wheel input and (b) vehicle sideslip angle as functions of vehicle lateral acceleration when driving through the steady-state constant radius maneuver using the path-following and speed-control driver models

the vehicle speed from 10 km/h to the maximum speed of 90 km/h in increments of 20 km/h. Next, the driver reduces the vehicle speed back to 10 km/h, again in a stepwise manner. Figure 15 illustrates the driver's speed request and the actual vehicle speed response for this maneuver. As can be seen, the actual vehicle velocity follows the driver's request very well, without causing any overshoot or significant over-damped conditions. Note that the torque of the in-wheel motors reduces as the vehicle drives faster as a result of the undesirable induction voltage produced by the permanent magnets. Consequently, the acceleration response at lower speeds is faster than that at higher speeds (Figure 15).

This effect is confirmed by Figure 16, which illustrates the motor torques during this maneuver. Note that, at the beginning and end of the test maneuver, where the vehicle is travelling at lower speeds, the maximum motor torque is available at each wheel; as the vehicle speed increases, the maximum possible motor torque decreases. It is important to notice that the slip controllers on the front axle have limited the motor torques at the beginning of the maneuver in order to avoid tire spin-out, and the slip controllers at the rear wheels have limited the motor torques at the end of the maneuver in order to avoid tire lock-up [3].

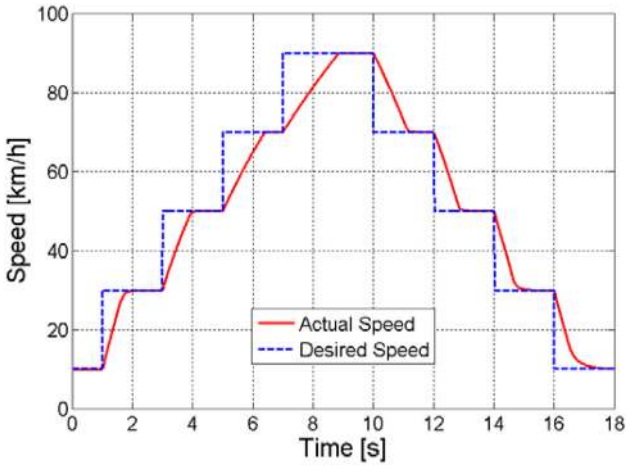

Figure 15. Stepwise speed request from the driver model and the actual speed of the vehicle

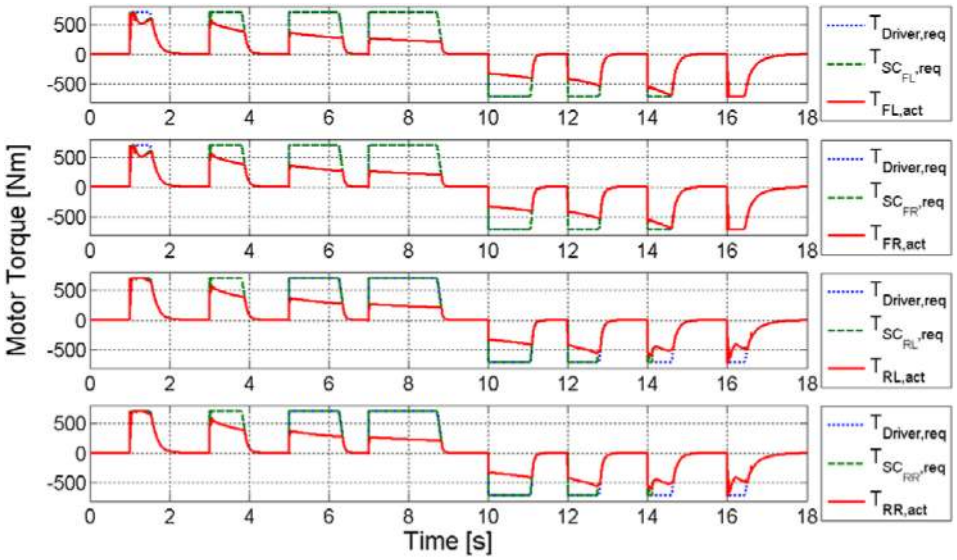

Figure 16. Motor torques during the stepwise speed variation test when driving in a straight line

CONCLUSION

In order to evaluate the handling and performance of the AUTO21EV, a two-passenger all-wheel-drive urban electric vehicle with four in-wheel motors and an active steering system, in the design stage and analyze the effectiveness of different chassis control systems before implementing them in the real vehicle, the simulation of a large number of different open-loop and closed-loop test maneuvers is necessary. In this regard, a moment-by-moment path-following driver model is developed in this work with an advanced path previewing technique. In addition, a gain scheduling speed control driver model is developed, which adjusts the drive torques of the wheels to minimize the deviation between the desired and actual vehicle speeds. The performance of the proposed path-following and speed control driver models are evaluated and confirmed using different test maneuvers.

ACKNOWLEDGMENTS

Funding for this work was provided by the Natural Sciences and Engineering Research Council of Canada and a grant from AUTO21, a Canadian Network of Centres of Excellence.

REFERENCES

1. Wallentowitz, H.: Vertical and Lateral Dynamics of Passenger Vehicles, Automotive Technology II, ("Vertical- und Querdynamik von Kraftfahrzeugen, Voerlesungsumdruck Fahrzeugtechnik II"), course notes, Institute of Automotive Engineering, Aachen University of Technology, Germany, 2005.
2. Bosch Automotive Handbook, 7th edition, Robert Bosch GmbH, Plochingen, 2007.

3. Jalali, K.: Stability Control of Electric Vehicles with In-wheel Motors, Ph.D. Thesis, University of Waterloo, 2010.

4. Roenitz, R., Braess, H.H., and Zomotor, A.: "Methods and criterions for evaluation of the behaviour of the passenger vehicle - Part I", (Verfahren und Kriterien zur Bewertung des Fahrverhaltens von Personenkraftwagen Stand und Problematik, Teil 1), ATZ Automobil-technische Zeitschrift, 1/77 and 3/77, pp. 29-38 and 39-46, 1977.

5. Roenitz, R., Braess, H.H., and Zomotor, A.: "Methods and criterions for evaluation of the behaviour of the passenger vehicle - Part II", ("Verfahren und Kriterien zur Bewertung des Fahrverhaltens von Personen-kraftwagen - Ein Rueckblick auf die letzten 20 Jahre, Teil 2"), ATZ Automobiltechnische Zeitschrift, 99/100, pp. 780-786, 1998.

6. Dixon, J.C., "Tires, Suspension, and Handling," SAE International, Warrendale, PA, ISBN 978-1-56091-831-8, 1996, doi:10.4271/R-168.

7. Guo, K. and Guan, H.: "Modeling of driver/vehicle directional control system", Vehicle System Dynamics, 22(3-4), pp. 141-184, 1993.

8. Oezguener, O., Uenyelioglu, K.A., and Hatipoglu, C.: "An analytical study of vehicle steering control", Proceedings of the 4th IEEE Conference on Control Applications, pp. 125-130, 1995.

9. Blundell, M. and Harty, D.: The Multibody Systems Approach to Vehicle Dynamics, Society of Automotive Engineers, 2004.

10. MacAdam, C.C. and Johnson, G.F.: "Application of elementary neural networks and preview sensors for representing driver steering control behavior", Vehicle System Dynamics, 25(1), pp. 3-30, 1996.

11. Sharp, R.S., Casanova, D., and Symonds, P.: "A mathematical model for driver steering control, with design, tuning and performance results", Vehicle System Dynamics, 33, pp. 289-326, 2000.

12. Ziegler, J.G. and Nichols, N.B.: "Optimum setting for automatic controllers", Transactions of the ASME, 65, pp. 756-765, 1942.

13. Karray, F.O. and de Silva, C.: Soft Computing and Intelligent Systems Design, Pearson Education Limited, 2004.

14. Vogt, H., Schmitke, C., Jalali, K., and McPhee, J.: "Unified modelling and real-time simulation of an electric vehicle", International Journal of Vehicle Autonomous Systems, 6(3-4), pp. 288-307, 2009.

15. Pacejka, H.B., "Tire and Vehicle Dynamics," SAE International, Warrendale, PA, ISBN 978-0-7680-1702-1, 2002, doi:10.4271/R-372.

16. Bode, K.H.: Preliminary Suspension Design and Stability Control Strategies for an Electric Vehicle with Four Independently Driven In-Wheel Motors, Project Thesis, University of Waterloo, 2006.